Techno-economic assessment of the novel Gas Switching Reforming (GSR) concept for gas-fired power production with integrated CO_2 capture

Shareq Mohd Nazir[a], Schalk Cloete[b], Olav Bolland[a], Shahriar Amini[a,b*]

[a]Department of Energy and Process Engineering, Norwegian University of Science and Technology, Trondheim, Norway

[b]SINTEF Materials and Chemistry, Trondheim, Norway

Abstract

The focus of this study is to carry out techno-economic analysis of a pre-combustion capture method in Natural Gas based power plants with a novel reactor concept, Gas Switching Reforming (GSR). This reactor concept enables auto thermal natural gas reforming with integrated CO_2 capture. The process analysed integrates GSR, Water Gas Shift (WGS), and Pressure Swing Adsorption (PSA) into a Natural Gas based combined cycle power plant. The overall process is defined as GSR-CC. Sensitivity studies have been carried out to understand the performance of the GSR-CC process by changing the oxygen carrier utilization and Steam/Carbon ratio in GSR. The net electrical efficiency of the GSR-CC lies between 45.1% and 46.2% and the levelised cost of electricity lies between 124.4 and 128.1 $/MWh (at European natural gas prices) for the parameter space assumed in this study. By eliminating the WGS step from the process, the net electrical efficiency improves to 47.4% and the levelised cost of electricity reduces to 120.7 $/MWh. Significant scope exists for further efficiency improvements and cost reductions from the GSR-CC system. In addition, the GSR-CC process achieves high CO_2 avoidance rates (> 95%) and offers the possibility to produce pure H_2 during times of low electricity demands.

*Corresponding author
Email: shahriar.amini@sintef.no
Telephone: +47- 46639721
Address: S. P. Andersens veg 15 B, Trondheim, 7031, Norway

Keywords: pre-combustion CO_2 capture; Gas Switching Reforming; Natural Gas Combined Cycle power plants; Techno-economic analysis.

Nomenclature

BEC	Bare Erected Cost
CCS	Carbon Capture and Sequestration
CF	Capacity Factor
CGC	Carbon Gasification with CO_2
CGS	Carbon Gasification with Steam
CLC	Chemical Looping Combustion
CLR	Chemical Looping Reforming
COCA	Cost of CO_2 Avoidance
CSTR	Continuous Stirred Tank Reactor
EPCC	Engineering Procurement and Construction Cost
FC	Fuel Cost
FCF	Fixed Charge Factor
FOM	Fixed Operating and Maintenance
GSR	Gas Switching Reforming
GT	Gas Turbine
HP	High Pressure
HR	Heat Rate
HRSG	Heat Recovery Steam Generator
HTS	High Temperature Shift
LCOE	Levelised Cost of Electricity
LP	Low Pressure
LTS	Low Temperature Shift
MC	Methane cracking
MP	Medium Pressure
NG	Natural Gas
OSMR	Overall Steam Methane Reforming
SMR	Steam Methane Reforming
SPECCA	Specific Energy Consumption for CO_2 Avoidance
ST	Steam Turbine

TCR	Total Capital Requirement
TOC	Total Overnight Cost
TPC	Total Plant Cost
VOM	Variable Operating and Maintenance
WGS	Water Gas Shift
η	Net Electrical Efficiency

1 Introduction

The major part of the world's energy demands is still dependent on fossil fuels. The electricity sector has achieved better supply diversification via nuclear and renewables, but fossil fuels still dominate the global electricity mix [1]. The share of Natural Gas (NG) towards electricity generation has significantly increased in the last few decades because NG based power plants not only possess higher net electrical efficiency but also emit less CO_2 to the atmosphere when compared to coal based power plants [1]. This expansion is expected to continue over coming decades, with global NG consumption increasing by 50% between 2014 and 2040 according to the central scenario in the latest IEA World Energy Outlook [2].

Despite the lower emissions of NG power plants, broad deployment of CO_2 Capture and Sequestration (CCS) will still be required to meet the targets set at the COP 21 meeting in 2015. Natural gas based power plants with CCS will contribute substantially during the middle of the 21st century to meet COP 21 goals [3]. For perspective, the expected generation from CCS power plants by 2050 is about double the current generation from nuclear power.

Three specific methods for CCS have been researched upon and reported in literature: post-, oxy- and pre-combustion capture. A detailed review of these methods have been presented by Boot-Handford, Abanades [4] and Kenarsari, Yang [5]. The current paper focusses on a pre-combustion capture method using Gas Switching Reforming (GSR) in a NG based power plant.

Among the studied pre-combustion CO_2 capture methods, chemical looping systems present a potential of higher techno-economic performance [6]. The two most studied chemical looping concepts are Chemical Looping Combustion (CLC) [7] where the chemical potential of the NG fuel is converted to thermal energy, and Chemical Looping Reforming (CLR) [8] where the chemical potential of NG is converted mainly to chemical potential of a syngas fuel, which can be further converted to hydrogen. Both these concepts can achieve CO_2 capture with minimal energy penalties, but are hampered by challenges related to scaling up of the interconnected reactors and external circulation of oxygen carrier, especially under the pressurized conditions required for high efficiency. To address these challenges, a novel fluidized bed reactor concept involving gas switching has been demonstrated experimentally for combustion and reforming [9, 10]. The principle behind gas switching is similar to the operating strategy first utilized in

packed bed chemical looping combustion [11] and, more recently, in packed bed chemical looping reforming [12].

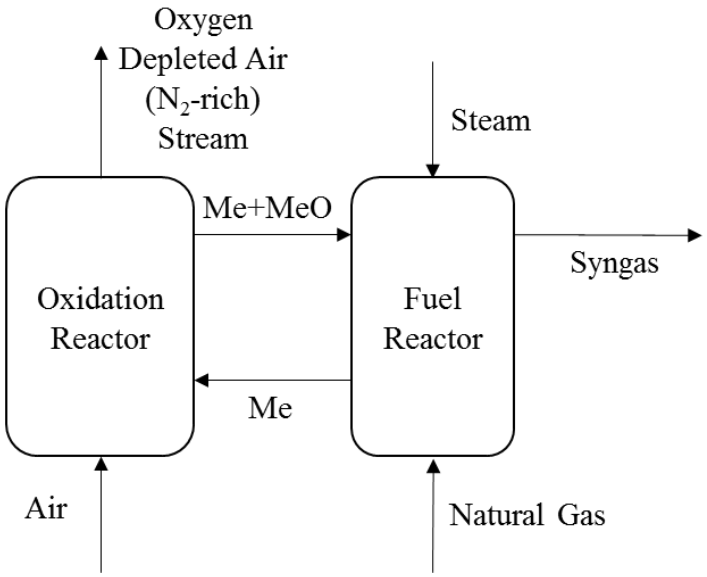

Figure 1: Chemical looping reforming (CLR)

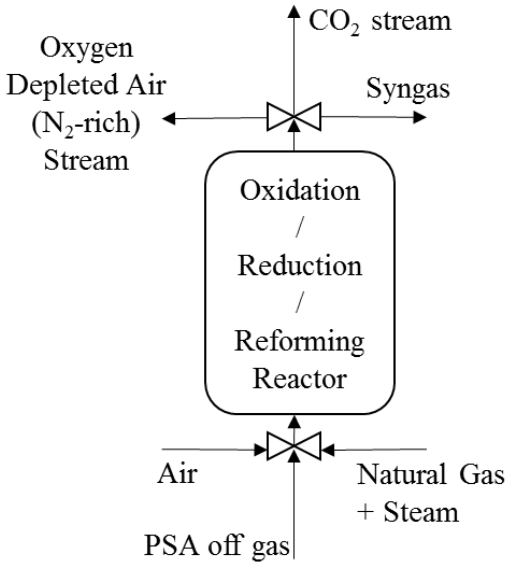

Figure 2: Gas switching reforming (GSR)

Figure 1 and Figure 2 show the schematic of the CLR and GSR respectively. CLR comprises of an interconnected oxidation and fuel reactor, with the metal oxygen carrier circulating between them. The metal oxygen carrier is oxidized with air in the oxidation reactor to give a metal oxide stream, alongside a depleted air stream containing mainly N_2. The metal oxide then reacts with the fuel in presence of steam in the fuel reactor to produce syngas and regenerate the metal oxygen carrier.

On the other hand, GSR operation keeps the oxygen carrier inside one reactor with alternate switching of gaseous streams during each step of oxidation, reduction and reforming. The metal

oxygen carrier is first oxidized in the oxidation step with air, leaving metal oxide in the reactor while producing a N_2-rich stream. The metal oxide is then reduced to metal during the reduction step by a fuel gas, yielding a high purity CO_2 stream after steam is separated out. The reduced metal, heated to a high temperature by the combustion of fuel gas, then acts as a catalyst and heat supplier for the endothermic steam-methane reforming during the reforming step. Hence, metal circulation is avoided in the GSR, but the dynamic nature of this operating strategy requires a cluster of multiple reactors operating in a coordinated manner to create a suitably steady state process unit.

Another interesting feature of GSR when compared to CLR is that the reduction and reforming steps are separated. This allows for efficient integration of a Pressure Swing Adsorption (PSA) unit for high purity hydrogen production [13]. Specifically, the carbon-rich off-gases from the PSA unit can be fed back to the GSR reduction step where it is combusted to yield a high-purity CO_2 stream for storage or utilization. The possibility of efficient integration of a PSA unit promises increased CO_2 capture rates and the potential for the GSR integrated combined cycle power plant to sell high purity hydrogen instead of electricity during times when the electricity price is low.

Furthermore, GSR reactors are much better suited to flexible operation than CLR reactors. Since GSR reactors are simple standalone bubbling fluidized beds, the gas flowrate can be varied over more than an order of magnitude without any serious problems. CLR reactors, on the other hand, must operate in a narrow fluidization window to maintain reliable oxygen carrier circulation. These features of power plant with GSR could greatly increase its attractiveness in a future market with high CO_2 prices, volatile electricity prices due to variable wind/solar power generators, and potentially large hydrogen demand from fuel cell vehicles.

With respect to chemical looping systems, scientific literature is available on development and choice of oxygen carrier [6, 14], reactor scale modeling and experimental studies [8, 13, 15-21]. Integration of pre-combustion methods with gas fired power plants and techno-economic assessment has been reported in literature [22-29]. Analysis of the combined cycle power plants with chemical looping reforming (CLR-CC) have been reported with a net electrical efficiency of the CLR-CC process between 42-46% [30, 31]. With respect to the gas switching concept, experimental demonstration [9, 10] and 1-D modeling studies [13] have been reported in literature. Integration of the gas switching combustion system in Integrated Gasification Combined Cycle (IGCC) process yields a net electrical efficiency of 5 % points more than the baseline IGCC plant with CO_2 capture [33].

The techno-economic performance of the GSR concept has not yet been studied. As outlined earlier, the separation of reduction and reforming steps in the GSR concept requires a different plant layout than the CLR based power plant [30, 31]. Specifically, the power plant integrated with CLR and CO_2 capture utilizes a chemical absorption method to capture CO_2 from the CLR syngas stream. Imperfect CO_2 capture and any unconverted CH_4 or CO directly result in CO_2 emissions from the CLR based combined cycle power plant. In contrast, GSR can efficiently utilize a PSA unit for pure hydrogen separation resulting in zero emissions from the gas turbine. Any carbon-containing gases are directly recycled back to the GSR reduction step and converted to a pure stream of CO_2 and H_2O via oxygen carrier reduction. The potential advantages in terms of process efficiency, CO_2 capture rate and electricity cost offered by integrating the GSR concept with a PSA unit will therefore be quantified in this study. To

summarize, the novelty of this study will be a techno-economic assessment of a novel pre-combustion capture process configuration with GSR in NG based combined cycle power plants. The integrated process will be referred to as GSR-CC hereafter. The GSR-CC process combines GSR, Water Gas Shift (WGS), and PSA, followed by a combined cycle power plant that uses H_2-rich fuel in the gas turbine system. The effect of design conditions in GSR like the cycle time and steam/carbon ratio on the overall techno-economic performance of the GSR-CC process is estimated and reported. The process is also analysed without the WGS step. Net electrical efficiency, CO_2 avoidance, Cost of CO_2 Avoidance (COCA) and Levelised Cost of Electricity (LCOE) have been identified as the techno-economic performance indicators. The remaining part of the paper contains description of the process, methodology, results and discussion followed by conclusions.

2 Process Description

Figure 3 shows the schematic of the GSR-CC process. During the GSR oxidation step, compressed air at 18 bar is reacted with metal oxygen carrier (Ni supported on alumina). Essentially all the oxygen in the air is consumed due to the high reactivity of the oxygen carrier, which is generally kept in a reduced state (high availability of Ni for reaction with O_2). The resulting N_2-rich stream from the oxidation step is expanded in the N_2-rich stream turbine to produce power. After expansion, the N_2-rich stream is cooled down by producing saturated High Pressure (HP) steam at 174.4 bar and pre-heating the H_2-rich fuel to the Gas Turbine (GT). A fraction of the cooled N_2-rich stream (equal to the amount of air bleed from the GT) is compressed in two stages and used as a diluent in the GT system. Inter-stage cooling of the N_2-rich stream is done by producing saturated HP steam (174.4 bar). The pressure of the saturated HP steam produced while recovering heat is based on the design of the heat recovery steam generator in the power plant section. The proposed process scheme to treat the N_2-rich stream is similar to the work in Nazir, Bolland [30].

Subsequently, the metal oxide from the oxidation step is reduced with the off gas from PSA. Additional NG (assumed 100% CH_4 in this study) is mixed with the PSA off gas in the reduction step to completely reduce the metal oxide. Hence, the gaseous product stream from the reduction step contains mainly CO_2 and H_2O, which is cooled to produce saturated HP steam (174.4 bar) and then condensed before the CO_2 stream is compressed and made ready for transport and storage. The hot reduced oxygen carrier remaining in the reactor after the reduction step acts as the catalyst and heat source for steam methane reforming during the reforming step. The steam required during the reforming stage is extracted from the Medium Pressure (MP) turbine in the Steam Turbine (ST) cycle. Syngas is produced as the product from the reforming step.

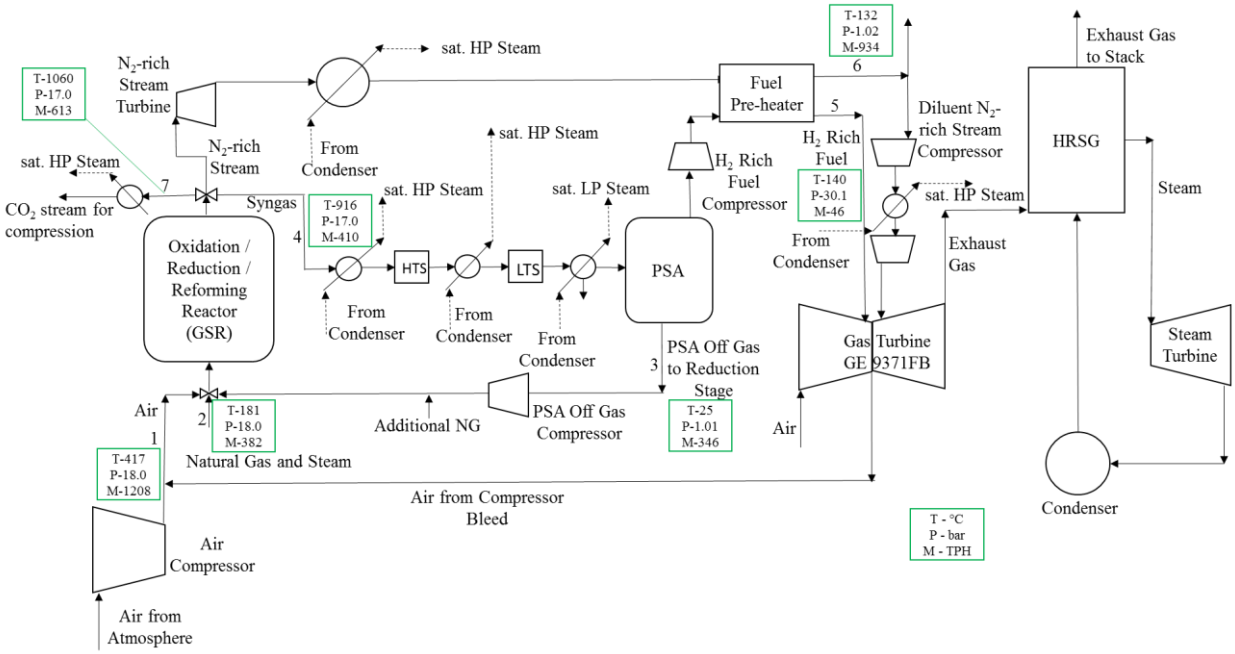

Figure 3: Schematic of a GSR-CC process

Table 1: Process stream data for Case 2 (Oxygen carrier utilization - 35%, S/C ratio - 1.5)

Stream	Flow (TPH)	T (°C)	P (bar)	Mole Composition (%)							
				H_2O	CO_2	CH_4	CO	H_2	N_2	O_2	Ar
1	1208	417	18.00	1.03	0.03	0.00	0.00	0.00	77.29	20.73	0.92
2	382	181	18.00	60.0	0.00	40.0	0.00	0.00	0.00	0.00	0.00
3	346	25	1.01	2.51	44.88	9.31	13.85	28.68	0.76	0.00	0.01
4	410	916	17.00	15.06	4.25	3.29	16.47	60.65	0.27	0.00	0.00
5	46	140	30.11	0.00	0.00	0.01	0.00	99.99	0.00	0.00	0.00
6	934	132	1.02	2.82	0.65	0.00	0.00	0.00	95.40	0.00	1.13
7	613	1060	17.00	46.09	51.18	0.00	0.00	0.00	2.69	0.00	0.03

The syngas from the reforming step in the GSR is cooled and subjected to High Temperature (HTS) and Low Temperature (LTS) WGS reaction to convert CO and H_2O into CO_2 and H_2. Saturated HP steam (174.4 bar) is produced while cooling the syngas and HTS product. The LTS product is cooled and is sent to PSA to separate H_2 from the mixture. Saturated Low Pressure (LP) steam is produced while cooling the LTS product. The PSA separates the H_2 from the mixture and gives a H_2-rich stream that acts as GT fuel in the power plant. The PSA also gives an off gas stream which contains a mixture of H_2, CO_2, CO, CH_4 and H_2O. The off gas stream from PSA is compressed, mixed with additional NG stream, and sent to the GSR during the reduction step. The H_2-rich stream from the PSA is compressed and pre-heated before being used in the GT system.

The power plant is a combined cycle with two GTs, two Heat Recovery Steam Generators (HRSG), and one Steam Turbine (ST). The power plant configuration is similar to the combined cycle configuration of the reference Natural Gas Combined Cycle (NGCC) plant without CO_2 capture described in the European Benchmarking Task Force report [34]. Similar power plant configuration have also been used in the analysis of the CLR-CC process [30, 31]. The H_2-rich fuel is combusted with compressed air in the GT system. N_2-rich stream is added as a diluent to the GT system along with the H_2-rich stream. The hot exhaust gas from the GT system is used to produce steam for the steam cycle in the power plant. The steam cycle is a three pressure level cycle and comprises of a reheat for the Medium Pressure (MP) steam, with one HP turbine, one MP turbine and two flow LP turbines. The corresponding three pressure levels are 3.4/32.7/166 bar for LP/MP/HP steam respectively. The saturated HP and LP steam produced in the process from cooling of process streams like N_2-rich stream, syngas, HTS product, CO_2 stream from reduction step in GSR and LTS product is sent to the respective HP and LP superheaters in the HRSG. The water and the steam mixture from the ST system is condensed in a water-cooled condenser. The condensed water is pumped and sent to the HRSG. The cooling water requirements in the entire process is satisfied by one natural draft cooling tower. The methodology section describes the assumptions made while analyzing the GSR-CC process.

3 Methodology

3.1 Reactor modelling

The GSR reactor was modelled as a Continuous Stirred Tank Reactor (CSTR), which is generally a good assumption for a well-mixed fluidized bed. In addition, thermal and chemical equilibrium was assumed. Thermal equilibrium is easily achieved in fluidized beds due to the very fast gas-particle heat transfer resulting from the dynamic mixing and small particle size. Chemical equilibrium is also a good assumption due to the highly active Ni-based oxygen carrier employed. Earlier 1D model simulations of a CLR fuel reactor showed that reactor length (gas residence time) had a very small influence on reactor performance because the fast reactions quickly reach equilibrium [13]. More importantly, a recent experimental demonstration of the GSR concept showed that chemical equilibrium is reached even in a small lab-scale reactor [9]. The CSTR model assuming thermal and chemical equilibrium will therefore deliver sufficiently accurate predictions of a large-scale GSR reactor where the gas residence time is much longer than the aforementioned lab-scale demonstration study.

Subsequent sections provide more details on the reactor model, highlight typical model outputs, and discuss the connection between reactor and power plant modelling.

3.1.1 GSR reactions

Four heterogeneous and three catalytic reactions are simulated in the process. Eq. 1 - Eq. 3 mainly take place in the reduction step, Eq. 4 in the oxidation step, and Eq. 5 - Eq. 7 in the reforming step.

$$CH_4 + 4NiO \rightarrow 4Ni + CO_2 + 2H_2O \qquad R_1 = \frac{1}{\tau} N_{CH_4} N_{NiO} \qquad \textit{Eq. 1}$$

$$H_2 + NiO \rightarrow Ni + H_2O \qquad R_2 = \frac{1}{\tau} N_{H_2} N_{NiO} \qquad \textit{Eq. 2}$$

$$CO + NiO \rightarrow Ni + CO_2 \qquad R_3 = \frac{1}{\tau} N_{CO} N_{NiO} \qquad \textit{Eq. 3}$$

$$O_2 + 2Ni \rightarrow 2NiO \qquad R_4 = \frac{1}{\tau} N_{O_2} N_{Ni} \qquad \text{Eq. 4}$$

$$CH_4 + H_2O \leftrightarrow CO + 3H_2 \qquad R_5 = \frac{1}{\tau}\left(p_{CH_4} p_{H_2O} - \frac{p_{CO} p_{H_2}^3}{K_{SMR}}\right) \qquad \text{Eq. 5}$$

$$CO + H_2O \leftrightarrow CO_2 + H_2O \qquad R_6 = \frac{1}{\tau}\left(p_{CO} p_{H_2O} - \frac{p_{CO_2} p_{H_2O}}{K_{WGS}}\right) \qquad \text{Eq. 6}$$

$$CH_4 + 2H_2O \leftrightarrow CO_2 + 4H_2 \qquad R_7 = \frac{1}{\tau}\left(p_{CH_4} p_{H_2O}^2 - \frac{p_{CO_2} p_{H_2}^4}{K_{OSMR}}\right) \qquad \text{Eq. 7}$$

Very fast reaction rates (R [kmol/s] in Eq. 1 - Eq. 7) are implemented to attain the equilibrium conditions by setting $\tau = 0.001$. N [kmol] is the total species in the reactor and p [bar] is the species partial pressure. As is evident from the equations, Eq. 1 - Eq. 4 are assumed to proceed until one of the reactants is consumed, while Eq. 5 - Eq. 7 proceed to the equilibrium conditions as proposed by Xu and Froment [35] (Eq. 8 - Eq. 10).

$$K_{SMR} = 1.2 \times 10^{13} \exp\left(\frac{-223080}{RT}\right) \qquad \text{Eq. 8}$$

$$K_{WGS} = 0.0177 \exp\left(\frac{36580}{RT}\right) \qquad \text{Eq. 9}$$

$$K_{OSMR} = 2.124 \times 10^{11} \exp\left(\frac{-168000}{RT}\right) \qquad \text{Eq. 10}$$

The possibility of carbon deposition was also investigated. It has long been known that carbon deposition can take place on a Ni catalyst [36], which could lead to catalyst deactivation as well as decreased CO_2 capture efficiency of the GSR-CC process. Three additional Ni-catalyzed reactions were therefore considered as follows based on the work of Snoeck et al. [37, 38]:

$$CH_4 \leftrightarrow C + 2H_2 \qquad K_{MC} = exp\left(\frac{116}{R}\right) exp\left(\frac{-101000}{RT}\right) \qquad \text{Eq. 11}$$

$$CO_2 + C \leftrightarrow 2CO \qquad K_{CGC} = exp\left(\frac{178}{R}\right) exp\left(\frac{-169000}{RT}\right) \qquad \text{Eq. 12}$$

$$H_2O + C \leftrightarrow CO + H_2 \qquad R_{CGS} = \frac{K_{CGC}}{K_{WGS}} \qquad \text{Eq. 13}$$

A simple equilibrium calculation was then performed with six equilibrium reactions (Eq. 5 - Eq. 7 and Eq. 11 - Eq. 13). Calculations were completed at different CH_4:H_2O ratios, different temperatures relevant to the GSR process and a pressure of 18 bar. The fraction of carbon in the incoming CH_4 deposited as solid C at equilibrium was then plotted in Figure 4.

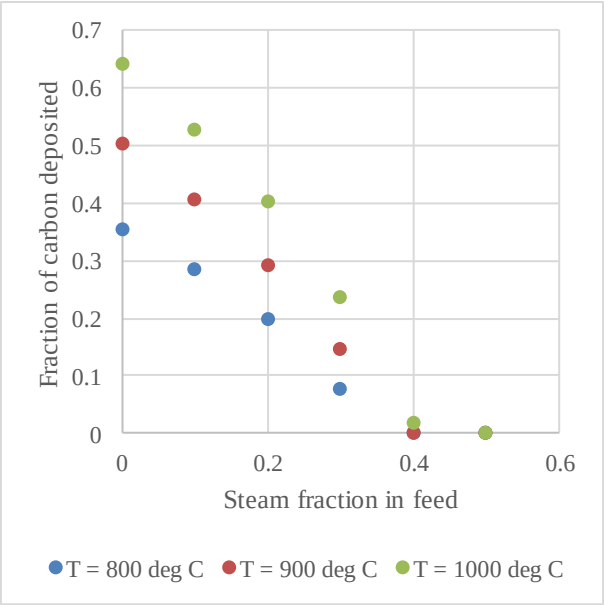

Figure 4: Fraction of incoming carbon deposited as solid C at equilibrium under different feed compositions and temperatures at a pressure of 18 bar.

Under the assumption that the GSR reactor is large enough to reach equilibrium, Figure 4 shows that carbon deposition will be insignificant as long as the steam/carbon ratio of the feed gas is greater than 1. Carbon deposition is mostly observed in fixed bed reactors (for example Iliuta, Tahoces [39]) where the plug flow nature of the reactor can result in significant carbon deposition at higher steam/carbon ratios if the reaction rate of Eq. 11 is significantly faster than Eq. 12 and Eq. 13. However, in a large well-mixed fluidized bed operating at relatively high temperatures, the complete chemical equilibrium assumption is reasonable and carbon deposition is not expected to pose a significant problem. Given that this study will not use steam/carbon ratios lower than 1, carbon deposition (Eq. 11 - Eq. 13) will not be included in the reactor simulations.

3.1.2 Mole and energy balances

The following mole and energy balances are solved using the 'ode15 differential-algebraic' equation solver in Matlab.

$$\frac{dN_{g,i}}{dt} = F_g^{in} y_{g,i}^{in} - F_g y_{g,i} + \sum_k s_{i,k} R_k \qquad \text{Eq. 14}$$

$$\frac{dN_{s,j}}{dt} = \sum_k s_{j,k} R_k \qquad \text{Eq. 15}$$

$$\left(\sum_i N_{g,i}\, C_{P,i} + \sum_j N_{s,j}\, C_{P,j} \right) \frac{dT}{dt} = \sum_i \left(F_g^{in} y_{g,i}^{in} h_{g,i}^{in} - F_g y_{g,i} h_{g,i} \right) + \sum_k R_k \Delta H_k^R \qquad \text{Eq. 16}$$

In the gas species mole balance (Eq. 14), $N_{g,i}$ [kmol] is the gas holdup of gas species i. F_g^{in} and F_g [kmol/s] are the total molar flowrates into and out of the reactor respectively. The final term is the source term due to the different reactions, where $s_{i,k}$ is the stoichiometric constant of species i in reaction k and R_k [kmol/s] is the rate of reaction k. The solids mole balance (Eq. 15) is similar for each species j, but there is no inflow or outflow of the material.

Eq. 16 shows the energy balance, where $C_{P,i}$ and $C_{P,j}$ [J/kmol.K] are the heat capacities of gas species i and solids species j respectively. T [K] is the temperature, while $h_{g,i}^{in}$ and $h_{g,i}$ [J/kmol] are the enthalpies of incoming and outgoing gas species i. All heat capacities and enthalpies are calculated as a function of temperature based on gas species data from Stull and Prophet [40] and solids species data from Robie and Hemingway [41]. ΔH_k^R [J/kmol] is the reaction enthalpy of reaction k.

Finally, the ideal gas law is used to specify the number of gas moles in the reactor.

$$PV_g = \sum_i N_i R_0 T \qquad \textit{Eq. 17}$$

Here, P [Pa] is the pressure, V_g [m^3] is the gas volume (difference between reactor volume and solids volume), and R_0 [J/kmol.K] is the universal gas constant.

3.1.3 Initial and boundary conditions

Inlet gas stream flowrates, temperatures and compositions to the different process steps were case-dependent. However, the inlet and outlet pressures were fixed to 18 and 17 bar respectively (1 bar pressure drop over the reactor). The reactor was specified to be 10 m in height and 6.7 m in in diameter and filled with oxygen carrier to yield a total reactor void fraction of 0.65. The oxygen carrier density was set to 4000 kg/m^3 in its initial fully reduced state, with a Ni mass fraction of 0.3 and the balance Al_2O_3 support material.

Gas feed rates were specified to keep the superficial velocity through the reactor around 0.5 m/s to facilitate bubbling fluidization. The duration of the different steps in the GSR process was adjusted based on the degree of oxygen carrier utilization specified, but a ratio of oxidation:reduction:reforming duration of 2:1:2 was always maintained to enable steady operation with a GSR reactor cluster containing any multiple of 5 reactors.

3.1.4 Reactor behavior and link to process model

This section will present some typical reactor model outputs and describe how these results are then incorporated in the process and power plant modelling. The basic behavior of the GSR reactor is illustrated in Figure 5. During the reduction step, all the incoming fuel gases are converted to CO_2 and H_2O and the reactor temperature slowly reduces, mostly due to the necessity to heat up the incoming fuel gases.

At the start of the reforming step (300 s in Figure 5), some remaining NiO must still be reduced and the incoming CH_4 is therefore converted to H_2O and CO_2. Some NiO is purposefully left at the end of the reduction step to account for the fact that the reduction reaction rates will slow down as the oxygen carrier comes close to full conversion, potentially leading to some undesired fuel slip. After this brief initial period of complete oxygen carrier reduction, the reforming reactions take place, producing H_2 and CO. Due to the endothermic nature of the reforming reaction, the temperature drops faster than in the reduction step. As the reactor temperature reduces, the CH_4 conversion and H_2 production also decline due to less favorable thermodynamics.

Finally, the oxidation step starts (900 s in Figure 5) to oxidize the oxygen carrier and heat up the reactor. During the first few seconds of oxidation, some H_2 and CO left in the reactor are

converted to H_2O and CO_2. Following this brief period, the outlet gases comprise of almost pure N_2 as all the O_2 in the air is consumed by the oxidation reaction.

Figure 5 also illustrates some undesired mixing between N_2 and CO_2 before and after the oxidation step. This mixing is due to the CSTR assumption and will lower the CO_2 capture rate and CO_2 purity achieved by the system. Nevertheless, the CO_2 capture performance of the system remains very high as will be described in the results and discussion section.

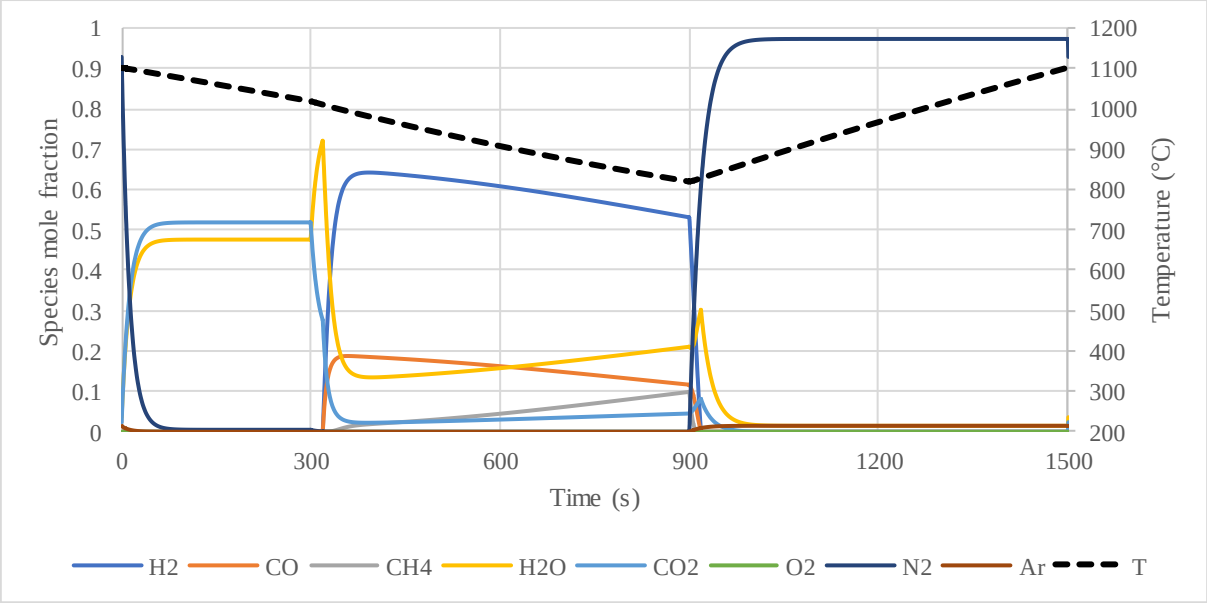

Figure 5: Reactor outlet gas species and temperature plot over one complete GSR cycle. The first 300 s of the cycle is reduction with PSA off-gas fuel, followed by 600 s of steam-methane reforming and 600 s of oxidation with air.

For linking to the process model, the outlet gas composition and temperature from each step of the reactor were averaged on the assumption that a cluster of GSR reactors will give a suitably steady state stream. This assumption was previously evaluated in more detail for the gas switching combustion (GSC) reactor concept [33], the combustion equivalent of GSR, showing that transient mass and temperature variations were sufficiently small to allow for steady operation of downstream equipment like a gas turbine. In the case of GSR, the reactor cluster will need to consist of a multiple of five reactors, alternatively running reduction, reforming and oxidation steps in a ratio of 1:2:2. The number of reactors should be determined by the temperature variations that can be tolerated by downstream process equipment: more reactors will yield steadier combined outlet streams. It should also be mentioned that the outlet streams were averaged assuming an 8 s delay in the outlet valve switch relative to the inlet valve switch. This practice increases the CO_2 separation performance of the reactor (more details in Cloete, Romano [33]).

The maximum reactor temperature was fixed at 1100 °C to protect the oxygen carrier material from thermal damages. This means that a longer cycle will allow the reactor temperature to drop to a lower level at the end of the reforming step, lowering the average outlet temperatures from all three reactor steps. The most important effect of this lower temperature in the GSR reactor is poorer CH_4 conversion in the reforming step. On the other hand, a longer cycle will also reduce the relative impact of the undesired mixing of N_2 and CO_2. This tradeoff between fuel conversion and N_2/CO_2 separation efficiency could potentially be minimized by adding a

steam purging step at the start and end of oxidation. Alternatively, the reactor could be designed with additional thermal mass (such as vertical metal bars) to reduce the temperature variation observed in Figure 5. In this case, however, it was found that such strategies were not required to achieve good process performance.

The resulting averaged outlet stream data was passed to the process models for WGS, PSA and the power plant. After this modification to the process model input, the off-gas stream from the PSA being fed to the reduction step of the GSR process is also changed. Following this update, the reactor model is run another time to give new output data to the process model for WGS, PSA and power plant. 4-5 such iterations were required to converge the connection between the reactor and process models.

3.2 Modeling Methodology and Assumptions

The air compressor, WGS, PSA off gas compressor, reduction step product cooling and CO_2 compression were modeled using Aspen Hysys V8.6 [42]. Peng-Robinson equation of state was used to estimate the thermodynamic properties in the process model. The composition and condition of atmospheric air is according to EBTF [34] report. The atmospheric air is compressed to 18 bar in the air compressor before being mixed with the compressed air bleed stream from the exit of the compressor in the GT system. The design pressure in the GSR unit, which is 18 bar, was selected because it is close to the pressure of the air bleed from the compressor discharge of the GT system. A design pressure of more than 18 bar will require an additional air compressor in the process scheme [30, 31]. 12% by mass of the total air inlet to the GT is bled at the compressor outlet of the GT and is used in the oxidation step in GSR. The polytropic efficiency of the air compressor is 90.9%.

The equilibrium reactor module in Aspen Hysys V8.6 was used to model the conditions in HTS and LTS. The inlet product streams to the HTS and LTS are at 400 °C and 200 °C respectively [30, 31, 43]. The pressure drop in both the WGS reactors is assumed to be 3%. The heat exchangers in the entire process have a pressure drop of 2% for gaseous streams, and 0.4 bar for liquid streams.

The PSA unit in this study was modeled as a “black box”. The purity of H_2 in the H_2-rich stream from the PSA unit is assumed 99.99% with 86% recovery of H_2 [44, 45]. The component balance around the PSA unit then leads to estimating the composition of the resulting outlet streams. The pressure of the H_2-rich fuel stream from the PSA unit is 0.2 bar less than the inlet stream whereas the temperature is 43 °C. The temperature is similar to the H_2-rich fuel temperature considered in the analysis of CLR-CC by Nazir, Bolland [30]. The off gas from the PSA is at atmospheric pressure and 25 °C. The PSA off gas is compressed to 18 bar before being mixed with additional NG and sent to the GSR reduction step. The work done in compressing the PSA off gas indirectly reflects the energy penalty in the PSA separation step. The additional NG stream is heated up to the temperature of compressed PSA off gas stream before it is mixed. The PSA off gas compressor has a polytropic efficiency of 90%. The flow rate of additional CH_4 to the reduction step in GSR is dependent on the amount of metal oxide remaining to be reduced. The product stream from the reduction step contains mainly CO_2 and H_2O. It is cooled and condensed before the CO_2 stream is compressed to 110 bar and is ready for transport and storage. The CO_2 compression cycle is similar to the one presented in EBTF [34]. The saturated HP steam produced while cooling syngas, HTS product, N_2-rich stream and reduction step product stream is at 174.4 bar. The saturated LP steam produced while cooling

LTS product stream is at 3.8 bar. The saturated steam pressures are based on the point at which they are being mixed with the other steam lines in the HRSG.

The combined cycle power plant along with the N_2-rich stream treatment has been modeled and analysed using the Thermoflex component of the Thermoflow Suite V26 [46]. Themoflow suite contains a database of the models of standard commercial GT systems. The N_2-rich stream is expanded in a N_2-rich stream turbine and cooled. A fraction of the N_2-rich stream, equivalent to the amount of the compressor bleed flow rate from the GT system, is compressed in two stages and used as diluent during the H_2-rich fuel combustion in the combustor of the GT [47]. The polytropic efficiency of the compressors used for compressing N_2-rich stream is 90%. The GT system considered in this study is GE-9371FB model as it exhibits robustness to the fuel types, especially to H_2-rich fuels [34, 48]. The power plant comprises of two GTs, two HRSGs and one ST system. The steam cycle consists of a three-pressure level with reheat before the MP turbine. The GT is run at full load conditions and the Lower Heating Value (LHV) input at the GT inlet is 1.55 GW in all the cases studied and presented in this paper. The net electrical efficiency (η), the CO_2 avoidance and the specific energy consumption for CO_2 avoided (SPECCA) are defined in Eq. 18, Eq. 19 and Eq. 20.

$$Net\ Electrical\ Efficiency\ (\eta) = \frac{100\ \times Net\ electricity\ produced\ in\ GSRCC\ process}{LHV\ of\ NG\ input\ to\ the\ process} \quad \textit{Eq. 18}$$

$$CO_2\ Avoidance\ (\%) = \frac{100\ \times\ (CO_2\ emitted\ in\ NGCC\ -\ CO_2\ emitted\ in\ GSRCC)}{CO_2\ emitted\ in\ NGCC} \quad \textit{Eq. 19}$$

$$SPECCA = \frac{HR - HRref}{\left\{\left(\frac{tCO_2}{MWh}\right) - \left(\frac{tCO_2}{MWh}\right)ref\right\}} \quad \textit{Eq. 20}$$

3.3 Economic analysis methodology and assumptions

The LCOE and COCA are the main economic performance indicators for the GSR-CC process. The methodology adopted to estimate the LCOE and COCA is proposed by GCCSI [49]. Eq. 21, Eq. 22 and Eq. 23 are used to calculate the LCOE and COCA. The definition of each term used in the equations is given in Table 2.

$$LCOE = \frac{(TCR)(FCF) + FOM}{(MW)(CF \times 8766)} + VOM + (HR)(FC) \quad \textit{Eq. 21}$$

$$FCF = \frac{r(1+r)T}{(1+r)T-1} \quad \text{Eq. 22}$$

$$COCA\left(\frac{\$}{tCO_2}\right) = \frac{LCOEGSRCC - LCOENGCC}{\left(\frac{tCO_2}{MWh}\right)NGCC - \left(\frac{tCO_2}{MWh}\right)GSRCC} \quad \text{Eq. 23}$$

Table 2: Definition of terms used in calculating LCOE.

Parameter	Definition	Unit
TCR	Total Capital Requirement in the base year of the analysis	$
FCF	Fixed Charge Factor as defined in Eq. 22	fraction
FOM	Fixed O&M costs	$/year
MW	Net power output of the plant	MW
CF	Capacity Factor – availability of the plant	Fraction
VOM	Variable O&M costs excluding the fuel costs	$/MWh
HR	Net power plant heat rate	MJ/MWh
FC	Fuel Cost per unit of energy	$/MJ
r	Interest or discount rate	%
T	Economic lifetime of the plant relative to its base year	years

The interest rate "*r*" and the economic lifetime of the plant is considered as 10% and 30 years in this study. The methodology to estimate the Total Capital Requirement (TCR) of the GSR-CC process is shown in Table 3. The Engineering Procurement Construction Costs (EPCC), Process and Project Contingency have been assumed considering that the GSR-CC technology is in an advanced state of maturity [49].

Table 3: Methodology to estimate the TCR of GSR-CC process.

Component	Definition
Bare Erected Cost (BEC)	Sum of installed cost of equipment
Engineering Procurement Construction Costs (EPCC)	8% of BEC
Process Contingency	10% of BEC
Project Contingency	15% of (BEC +EPCC + Process Contingency)
Total Contingencies	Process Contingency + Project Contingency
Total Plant Costs (TPC)	BEC +EPCC + Total Contingencies
Owners Cost	20.2% of TPC [50]
Total Overnight Costs (TOC)	TPC + Owners Cost
Total Capital Requirement (TCR)	1.14*TOC [50]

The assumptions in estimating the Fixed and Variable Operating & Maintenance costs are listed in Table 4. The cost of NG considered is as per the European Industry standards in 2016 and the euro to US dollar conversion is considered 1.18 USD/euro. All the other costs in Table 4 are referred from the work of Spallina, Pandolfo [23]. The cost of adsorbent is assumed from an online e-commerce source [51].

Table 4: Assumptions for Fixed and Variable Operating & Maintenance Costs.

Fixed O&M Costs		
Operating Labor	1.7	M$
Maintenance, Support and Administrative Labor	2.5	% of TOC
Property Taxes	Included in insurance costs	
Insurance costs	2	% of TOC
Cost of NG (Fuel Cost)	9.83	$/GJ LHV
Variable O&M Costs		
Consumables		
Cooling Water Make Up Costs	0.39	$/m^3
Process Water Cost	2.22	$/m^3
Catalysts and Sorbent Replacement		
Oxygen Carrier cost	15	$/kg
WGS catalyst cost	15574	$/m^3
Adsorbent cost	1.1	$/kg [51]
Replacement Period	5	Years
CO_2 Transport and Storage Costs	11.12	$/ton CO_2
Emissions Tax (CO_2 tax)	27.22	$/ton CO_2

The Sizing and Economics tool in Aspen Hysys V8.6, and the PEACE component in Thermoflow provides the equipment costs of all process components except for PSA and GSR. The rationality of the costs obtained from Aspen Hysys V8.6 and Thermoflow is validated by comparing the LCOE of NGCC plant without capture (LCOE of ~67 $/MWh for a fuel cost of 6.75 $/GJ-LHV with 20 years lifetime of a NGCC plant) using the equipment costs from these commercial software against the LCOE of NGCC plant without capture reported by DOE/NETL [52]. The cost of PSA is taken from the report of Netzer [53]. The cost of GSR is calculated using the methodology described in Peters and Timmerhaus [54]. The weight of the reactor is calculated, and a reference cost similar to that of Fluidized Catalytic Cracker is used along with a capacity factor of 0.6 [23]. The GSR is assumed to have a height of 10 m and diameter of 6.7 m. The weight of the reactor is estimated to be 62508 lbs whereas the capital cost is 22.2 M$. The installation cost for the reactor is assumed to be 80% of its capital cost and hence the bare erected cost of each reactor is estimated to be 39.9 M$. A cluster of 10 standalone reactors is assumed to operate for the power plant in this study. A detailed reactor design would also account for the costs of high temperature valves and piping system [55], but a sensitivity study with respect to the characteristics and lifetime of the valves is not a part of this paper. Zero inflation rate for the costs have been assumed in this study.

4 Results and Discussion

The main results from the techno-economic analysis of the GSR-CC process and its comparison to the reference case NGCC plant without capture are shown in Table 6. Table 5 presents the design conditions in the GSR unit. Table 1 shows the process stream data for Case 2 where the oxygen carrier utilization is 35% and S/C ratio is 1.5. Figure 6 shows the contribution of different costs like Fuel Costs (FC), TCR, FOM and VOM to the LCOE, whereas Figure 7 shows the contribution of costs of different process sections to the BEC.

The penalty on the net electrical efficiency observed in the cases presented for GSR-CC in this study is ~ 11-13 %-points with respect to the reference case. Apart from the inherent losses due to reforming and water gas shift reactions, the energy penalty in the GSR-CC process comes from the additional process components with respect to the reference case.

Gross power production from the turbomachinery in the GSR-CC plants is similar to the reference case (around 59% of LHV input). At first glance, this is a counter-intuitive finding because the thermal energy in the streams exiting the GSR reactors is converted to work at lower temperatures than the reference case. For example, the CO_2-rich gases exiting the reduction step of the GSR reactors (stream 7 in Figure 3) are used to generate steam for powering the steam turbine, whereas all of the process gases power the combined cycle in the reference case. In addition, a significant amount of MP steam is extracted from the steam turbine for feeding the reforming stage of the GSR reactors. However, the expansion work that is lost through these mechanisms is compensated by additional energy input to the process streams though the compressors for air, diluent N_2-rich stream, PSA off gas, and H_2-rich fuel, ultimately creating a similar gross power output.

Another important energy penalty in the GSR-CC system is related to the practical requirements of the primary gas turbine. Firstly, the compressor for the diluent N_2-rich stream, required to prevent excessive NOx formation when combusting the H_2-rich fuel, consumes a significant amount of power (4.4% of LHV input). To generate this compressed N_2-rich stream at 30 bar, the outlet gases from the air stage of the GSR reactors (stream 6 in Figure 3) must first be expanded at a relatively low temperature (<1000 °C), resulting in less useful work compared to the reference case where all gases enter the primary gas turbine at temperatures exceeding 1400 °C. In addition, the H_2-rich fuel from the PSA unit must be further compressed for injection into the combustion chamber at an additional electricity consumption equivalent to 0.8 % of LHV input.

Ideally, no diluent would be added to the H_2-rich fuel, and the hot N_2-rich stream from the air stage of the GSR reactors would be fed directly to the combustion chamber to be heated up further before expansion. This arrangement would significantly increase efficiency and reduce the number of process units, but is not feasible with currently available gas turbines.

Additional energy penalties arise from the PSA off-gas and CO_2 compressors. As shown in Table 6, the electricity consumption from the pressure swing separation of H_2 amounts to 1.9 % of LHV input, whereas the further compression of the CO_2-rich stream for transport and storage imposes an additional 0.9 %-points in energy penalty.

The TCR for the GSR-CC process is 3 times more than the TCR of the reference case. As shown in Figure 7, the GSR reactors represent the largest single capital cost increase, but significant capital costs are also attributed to other plant components. In addition, the significant energy penalty also enforces larger plant components for a given electricity output. The LCOE for the GSR-CC process is higher than the reference case, since the GSR-CC encounters more fuel, capital and operating and maintenance costs. The substantial increase in FOM is primarily attributed to replacement costs of the GSR oxygen carrier. As a result of the significant increase in LCOE, the GSR-CC plants assessed in this study impose a CO_2 avoidance cost of 112-134 \$/ton CO_2 on top of the 27.22 \$/ton CO_2 emissions tax assumed.

To analyze the techno-economic performance of GSR-CC at different design conditions in GSR, for cases 1, 2 and 3 in Table 5, the Steam/Carbon ratio in the reforming step is kept constant whereas the cycle time in oxidation step is varied to result in oxidation of 25%, 35% and 45% of the available Ni during the oxidation step of the GSR reactors. This independent variable is henceforth called “oxygen carrier utilization”. In cases 2, 4 and 5, the oxygen carrier

utilization is kept constant at 35% and the Steam/Carbon ratio in reforming step is evaluated at levels of 1.5, 1.2 and 2. Case 6 shows the results for a GSR-CC process without the WGS step.

Table 5: Conditions in oxidation, reduction and reforming steps of GSR for different cases.

Cases	Units	1	2	3	4	5	6 (GSR-CC without WGS)
Oxidation step							
Oxygen carrier utilization	%	25	35	45	35	35	35
Outlet Temperature	°C	1011	977	946	978	976	980
Air flowrate	TPH	1214	1208	1194	1190	1216	1166
N_2-rich stream flowrate	TPH	938	934	924	920	941	900
Reduction Step							
Outlet temperature	°C	1071	1060	1047	1065	1056	1082
PSA off gas flowrate	TPH	337	346	362	348	341	317
Additional CH_4 flowrate	TPH	29	21	7	4	37	0.4
Reforming Step							
Steam/Carbon		1.5	1.5	1.5	1.2	2	1.6
NG Flowrate	TPH	134	142	154.5	158	127	159
Outlet Temperature	°C	970	916	871	929	928	949
H_2O/CO in syngas	mol/mol	0.76	0.92	1.18	0.59	1.43	0.88

Table 6: Main results from techno-economic analysis for GSR-CC process. Power generation and consumption of individual plant components are expressed as a percentage of fuel (LHV) input.

Cases	Units	Ref. case (NGCC without capture)	1	2	3	4	5	6 (GSR-CC without WGS)
Gas Turbine	% - LHV input	37.7	26.8	26.9	27.0	27.0	26.7	27.4
Steam Turbine	% - LHV input	21.9	24.3	24.0	23.7	24.2	23.5	25.0
N_2-rich Stream Turbine	% - LHV input		8.1	7.8	7.6	7.7	7.8	7.8
Diluent N_2 Stream Compressor	% - LHV input		- 4.4	- 4.4	- 4.4	- 4.4	- 4.4	- 4.3
H_2 rich fuel Compressor	% - LHV input		- 0.8	- 0.8	- 0.8	- 0.8	- 0.8	- 0.8
Air Compressor	% - LHV input		- 3.4	- 3.4	- 3.4	- 3.3	- 3.4	- 3.3
PSA off gas compressor	% - LHV input		- 1.9	- 1.9	- 2.0	- 2.0	- 1.7	- 2.2
CO_2 Compressors and Pump	% - LHV input		- 0.9	- 0.9	- 0.9	- 0.9	- 0.9	- 0.9
Heating of additional NG stream	% - LHV input		- 0.4	- 0.3	- 0.1	- 0.1	- 0.4	- 0.0
Auxiliaries	% - LHV input	- 1.3	- 1.3	- 1.2	- 1.2	- 1.2	- 1.3	- 1.3

Net LHV Input to process	MW	1513	2266	2261	2250	2253	2277	2215
Net Electrical Efficiency	% - LHV input	58.4	46.1	45.8	45.5	46.2	45.1	47.4
CO_2 Avoidance	%	-	95.2	96.2	96.6	96.1	96.2	96.4
CO_2 Capture	%	-	96.8	97.4	97.7	97.4	97.5	97.5
SPECCA	MJ/kg CO_2	-	5.1	5.2	5.3	5.0	5.6	4.4
Economic Analysis								
TCR	M$	676	2202	2230	2300	2336	2173	2133
LCOE	$/MWh	84.1	124.4	125.8	128.1	126.8	126.5	120.7
COCA	$/t$CO_2$	-	124.2	127.6	134.1	130.7	129.5	111.8

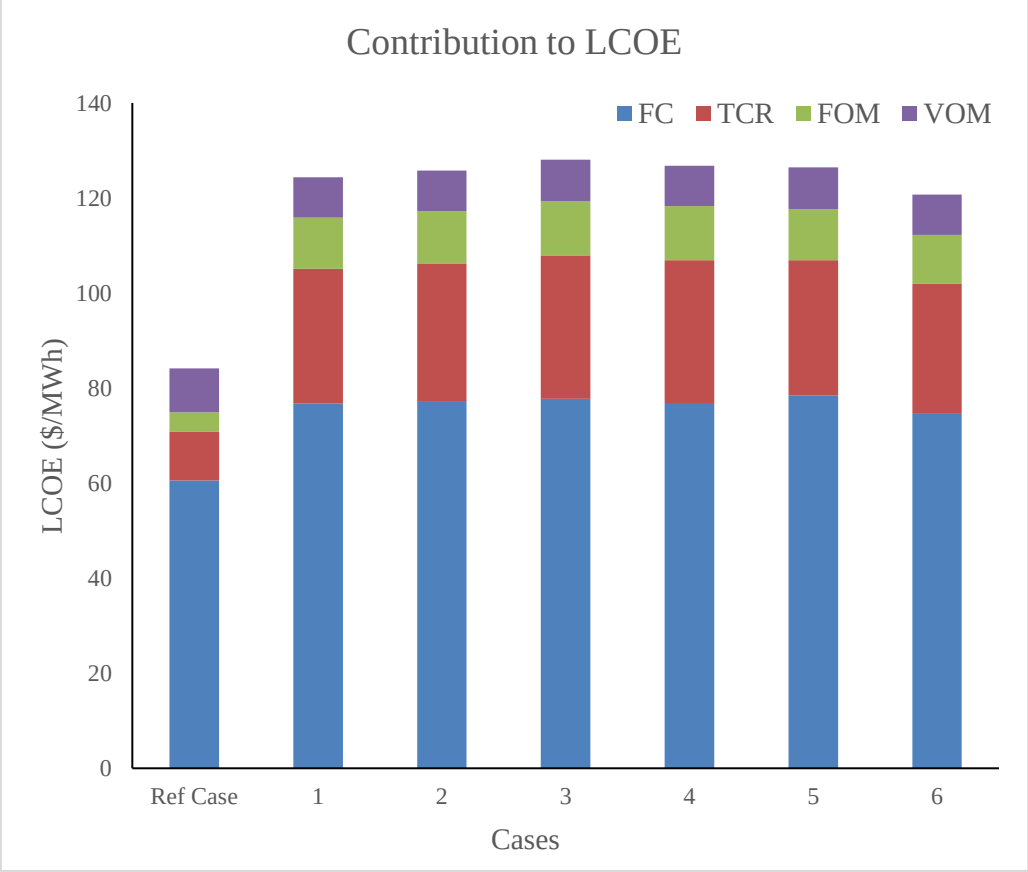

Figure 6: Contribution of different costs to LCOE.

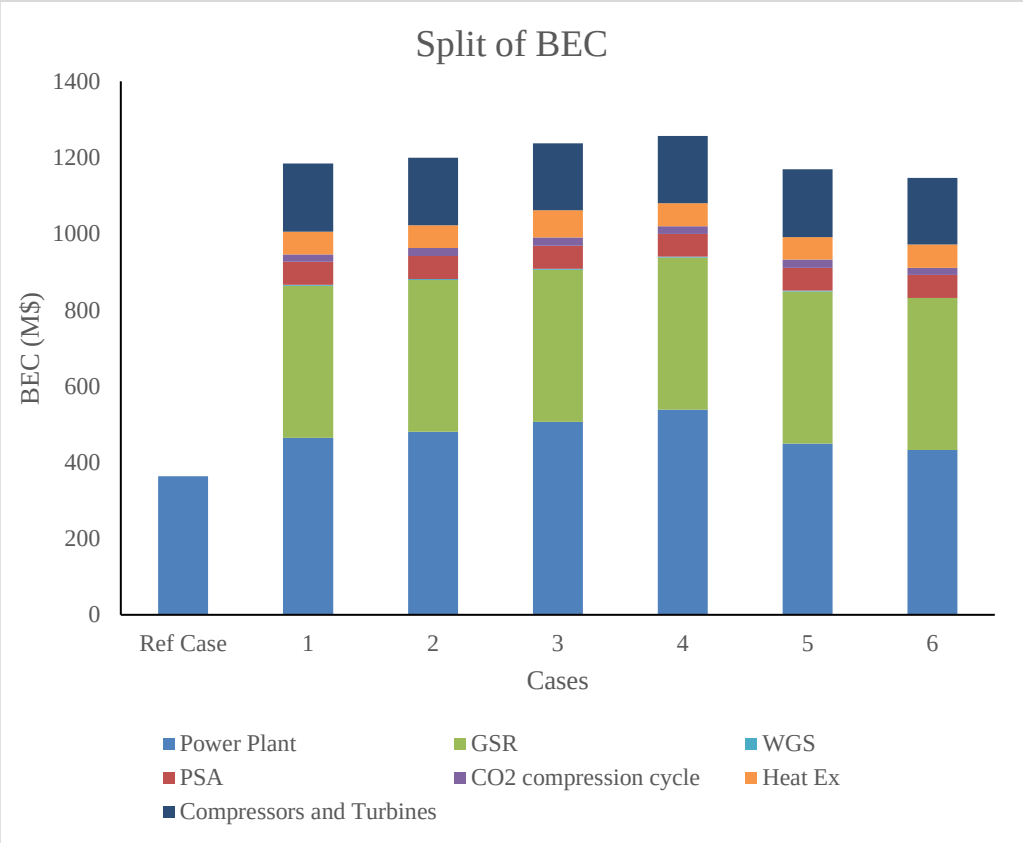

Figure 7: Contribution of different process sections to BEC

4.1 Effect of oxygen carrier utilization

The effect of oxygen carrier utilization is shown in cases 1, 2 and 3 in Table 5 and Table 6. An increase in oxygen carrier utilization increases the GSR cycle time, causing a greater temperature variation across the cycle (see Figure 5). Since the maximum reactor temperature is fixed to 1100 °C, such an increase in oxygen carrier utilization lowers the average temperature of all GSR outlet streams as can be observed in Table 5. As a result, the net electrical efficiency of the GSR-CC process decreases with an increase in oxygen carrier utilization since the work output from the steam turbine in the ST cycle and the N_2-rich stream turbine is reduced. The work output from the ST system depends on the amount of saturated HP steam, which is produced by cooling of process streams, sent to the HP superheater in the HRSG. In addition, the amount of steam extracted from the MP steam turbine for reforming is more when the cycle time is high because more NG is fed to the GSR reforming stage (Table 5). The work output from the N_2-rich stream turbine is directly related to the temperature of the N_2-rich stream from the oxidation step of the GSR. The effect of oxygen carrier utilization on power consumed by compressors and auxiliaries in the process is of lesser significance.

At higher oxygen carrier utilizations, the lower temperatures in the reforming step result in lower conversion of CH_4 and a higher H_2/CO ratio in the syngas. This results in NG flow rate to the reforming step being higher to produce the required amount of H_2-rich fuel for the GT system. However, the higher amount of unconverted CH_4 and CO is recycled back to the reduction stage of the GSR reactors, requiring a smaller addition of CH_4 to the PSA off gas. This is reflected in Table 5 where the flowrate of added CH_4 declines from 29 to 7 TPH when

the oxygen carrier utilization is increased from 25% to 45%. This also reduces the efficiency penalty considered due to heating up the additional NG stream to the temperature of the compressed PSA off gas.

The LCOE of the GSR-CC process increases with the degree of oxygen carrier utilization. This is due the higher heat rate (lower net electric efficiency) and the higher total capital requirement (TCR). As mentioned above, at higher oxygen carrier utilizations, the amount of saturated HP steam prepared from cooling of different process streams is less due to the lower logarithmic mean temperature difference (LMTD) between the process stream and the water stream that is being converted to steam. Lower LMTD between streams results in higher heat exchange area and costs (Figure 7). In addition, more saturated HP steam needs to be prepared from the HP boiler in HRSG. This results in HRSG of higher size and costs as shown in Figure 7.

CO_2 capture efficiency increases slightly with an increase in oxygen carrier utilization because the constant amount of undesired gas mixing when switching between stages (see Figure 5) becomes relatively smaller with longer cycle times. Despite this improvement, however, the Cost of CO_2 Avoidance (COCA) still increases with oxygen carrier utilization due the increase in LCOE.

4.2 Effect of Steam/Carbon ratio

Cases 2, 4 and 5 in Table 5 and Table 6 show the effect of Steam/Carbon ratio in the reforming step on the overall techno-economic performance of the GSR-CC process. The oxygen carrier utilization is kept constant at 35% for these cases and the Steam/Carbon molar ratio is assumed 1.5 in Case 2, 1.2 in Case 4, and 2 in Case 5. With different Steam/Carbon ratios in the reforming step of GSR, the temperatures in the oxidation step, reduction and reforming steps in the three cases do not vary much at a constant cycle time. However, the amount of NG reformed in GSR to produce the H_2-rich fuel for the GT system increases with Steam/Carbon ratio. This results in lower flowrates of PSA off gas stream and higher additional CH_4 flowrates when the Steam/Carbon ratio is high. Hence, less power is consumed by the PSA off gas compressor, but on the contrary, a higher efficiency penalty due to heating up of the additional NG stream.

The net electrical efficiency of the GSR-CC process is low when the Steam/Carbon ratio in the reforming step of GSR is high. The main difference in net electrical efficiency is due to the power produced from the ST cycle, power consumed by the PSA off gas compressor and the penalty due to heating up of additional NG stream. The primary reason for the trend of reduced steam turbine power output with increasing Steam/Carbon ratio is that it requires higher MP steam extraction from the ST.

The TCR is low when the Steam/Carbon ratio is high. The main cost impact is due to the cost of power plant section, which is low when the amount of saturated HP steam produced from heat recovery from process streams is high (Table 6). When steam produced by heat recovery from process streams is high, the size of the HP boiler in the HRSG system is low, and hence lower the cost of HRSG. Although, the size of heat exchangers used for heat recovery from process streams might increase, but it is also dependent on the LMTD in the heat exchanger. The LCOE of the GSR-CC process does not differ much in cases 2, 4 and 5 as lower TCR at high Steam/Carbon ratios is cancelled out by higher fuel costs (lower efficiency). Following the LCOE, the COCA is also similar between these three cases given that CO_2 avoidance was not significantly affected by Steam/Carbon ratio.

4.3 Effect of excluding WGS

The GSR-CC process was analysed without the WGS step, and the results are shown as Case 6 in Table 5 and Table 6. The oxygen carrier utilization is 35% and the Steam/Carbon ratio in the reforming step of GSR is 1.6. Under these operating conditions, there is negligible additional NG flowrate in the reduction step.

The net electrical efficiency for the GSR-CC process without a WGS step is high compared to the other cases described in this paper, because the inherent efficiency penalty due to WGS reactions does not exist. Hence, a higher conversion of the LHV input in GSR-CC to power produced from GT and ST in power plant is observed. The flowrate of PSA off gas is high which results in higher power consumption by the PSA off gas compressor. The PSA off gas flow rate is high because, in the absence of WGS step, the CO and H_2O in the syngas remain unreacted.

The TCR for the GSR-CC without WGS is lower as the cost of WGS reactors and the heat exchangers between the WGS steps is not included (Figure 7). The CO_2 avoidance and capture rate for GSR-CC without WGS is also more than 95% and 96% respectively. The LCOE for the GSR-CC without WGS is least among the cases studied in this paper, since the contribution of fuel costs and the TCR to the LCOE is less. Similarly, the COCA of Case 6 is the lowest for GSR-CC without WGS when compared to the GSR-CC cases with WGS.

4.4 Sensitivity to NG price

It is clear from Figure 6 that fuel cost is the major component of the LCOE. Hence, the LCOE of the GSR-CC process is very sensitive to the NG price. The NG price considered for the analysis above was 9.83 $/GJ-LHV which is the price in the European context (for the year 2014-2015), but there is a lot of variability of the price of NG around the world. Figure 8 shows the effect of NG price on the LCOE and COCA for the GSR-CC process without WGS (case 6). Clearly, lower NG prices substantially improve the economics of the process.

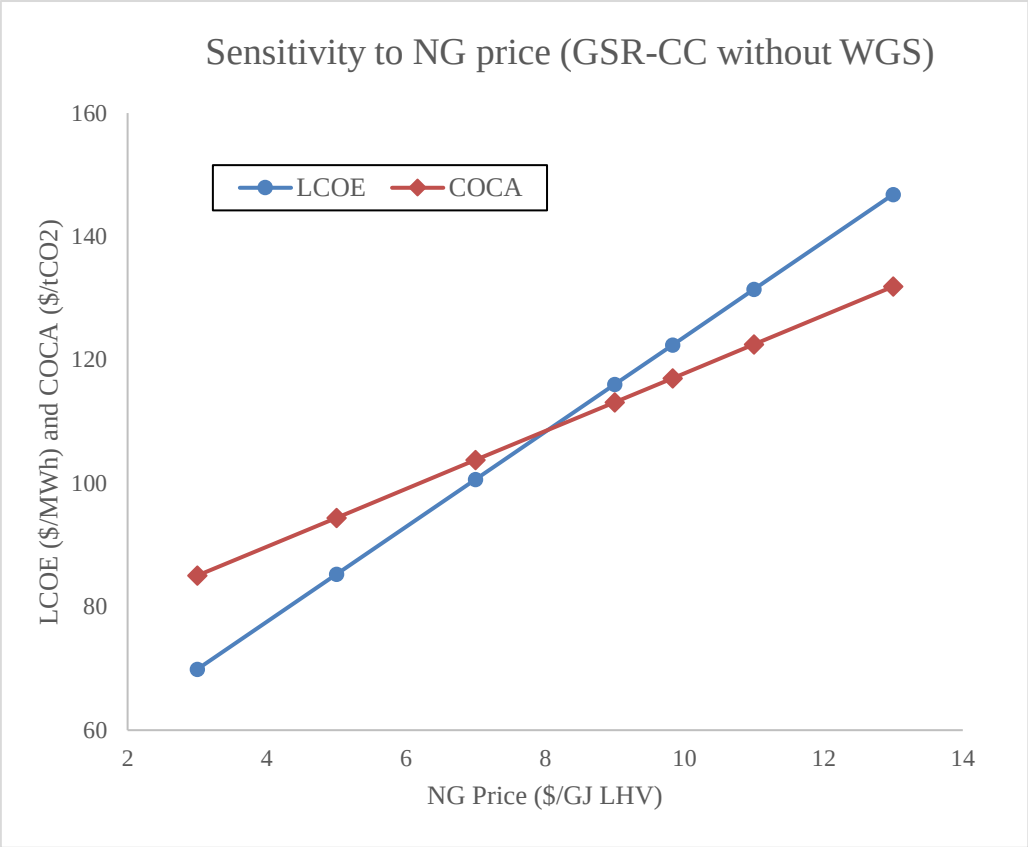

Figure 8: Sensitivity of LCOE and COCA to NG price for the case GSR-CC without WGS

5 Future outlook

The GSR-CC power plant investigated in this study will integrate well into the energy system of the future. Given the current emphasis on wind and solar power, flexibility of dispatchable power plants becomes increasingly important. As outlined in the introduction, the GSR-CC plant offers a high degree of flexibility both in terms of output (electricity or hydrogen production) and throughput (rate of electricity/hydrogen output). This capability will become increasingly desirable as electricity prices become more volatile with further wind/solar capacity expansion. In addition, the gas switching principle on which the GSR concept is based was primarily proposed to allow for rapid scale-up of chemical looping technology. In the event that policies consistent with the COP 21 targets are implemented in the medium-term future, this fundamental scalability can allow the GSR-CC to attract the investments required to achieve large-scale deployment.

To capitalize on this potential, further development of the GSR-CC concept is required. Firstly, significant efficiency advantages can be expected from advanced gas turbine technology utilizing lean premixed combustion to allow for no/minimal dilution of H_2 fuel with inert gases [56]. This will avoid the significant energy penalty and additional process units associated with low temperature expansion and recompression of the N_2-rich stream exiting the GSR reactor. Further optimization of heat integration strategies can allow for additional efficiency gains.

Secondly, oxygen carrier developments [57-59] can significantly reduce the expense related to the Ni-based oxygen carrier material considered in this study. Further studies on minimizing

the cost of the reactor can also lead to capital cost reductions. The present study calculates reactor costs based on an FCC benchmark, but it is possible that the standalone bubbling fluidized bed reactors employed in the GSR concept can facilitate significantly lower costs due to design simplicity and the use of cheaper refractory materials.

An important future challenge for the GSR technology is the requirement for high temperature valves and filters downstream of the reactors. This equipment needs to operate reliably at temperatures around 1000 °C, slightly above the upper limit of current market offerings. The GSR reactors can be operated at lower temperatures to avoid the need for new developments in downstream valves and filters, but this will result in lower fuel conversion in the reforming stage. Given that the GSR process can afford a certain level of unconverted fuel because the PSA off gas is efficiently utilized, the possibility of lower reactor temperatures to enable the use of currently available valves and filters is an interesting topic for future study.

The ability of a cluster of dynamically operated GSR reactors to create a steady-state processing unit also needs to be explicitly demonstrated. Given that several commercial processes in operation today employ this principle (e.g. the PSA process), this step is expected to be relatively straightforward.

In summary, the GSR-CC configuration introduced in this paper is 1) fundamentally suited to a future energy system with high wind/solar penetration, H_2 demand and CO_2 prices, 2) capable of achieving significant further cost reductions beyond the numbers reported in this study, 3) fundamentally designed for rapid scale-up, and 4) not hindered by serious technical challenges.

6 Conclusions

This paper focused on the process integration and techno-economic analysis of a novel pre-combustion CO_2 capture method in gas fired power plants, which uses the gas switching reforming (GSR) concept for efficient reforming of CH_4 with integrated CO_2 capture. The GSR concept is integrated into a combined cycle power plant and is therefore called GSR-CC. The GSR-CC process comprises of GSR, WGS, PSA for H_2 separation, CO_2 compression cycle and a H_2 fueled combined cycle power plant. The process has high flexibility with respect to the output (electricity or pure hydrogen) and throughput (rate of NG input).

The net electrical efficiency of the GSR-CC process is similar or higher than other combined cycle plants with pre-combustion capture like CLR-CC [30, 31] between 42-46 %, steam methane reforming at 43.65% [60] and auto-thermal reforming at 46.9 % [29]. The CO_2 avoidance observed in GSR-CC (>95%) is more than the other pre-combustion and post-combustion capture methods (~88%) [29]. Sensitivity analyses showed a slight efficiency increase (~1 %-point) when the oxygen carrier utilization and the S/C ratio are reduced. If WGS was removed from the GSR-CC process, the net electrical efficiency was observed to be ~2 %-points higher.

Although there exists advantages of GSR-CC over other capture methods especially with regard to efficiency and CO_2 avoidance, the TCR of GSR-CC is over 3 times the TCR of reference NGCC plant without capture. The primary capital cost increase comes from the reactor cost that is more than 30% of the total capital costs. Despite this large capital cost increase, fuel remains the primary cost component when European NG prices are used (9.83 $/GJ-LHV). In this case,

the increase in LCOE of the GSR-CC with respect to the LCOE of reference plant comes from the fuel cost (40% of the increase in LCOE), followed by the capital cost of the additional process equipment in GSR-CC (35% of the increase in LCOE) and the larger size of the process equipment due to efficiency penalty of the process (25% of the increase in LCOE). When the price of the NG is halved, the capital cost of the additional process equipment in GSR-CC becomes the primary cost increase (44% of the increase in LCOE), followed by costs due to larger equipment size because of efficiency penalty of the process (31% of the increase in LCOE) and fuel cost (25% of the increase in LCOE).

Given the large cost increase from fuel costs and larger sized process components caused by lower net electric efficiency, further efficiency improvements are highly desirable. Thermodynamic optimization was not in the scope of this study, but it is expected that the net electrical efficiency of the GSR-CC process can be improved substantially by detailed energy integration and optimization. Further work is recommended on this topic.

7 Acknowledgements

The authors thank the European Commission for the funding through the EU-FP7 framework for the project NanoSim (project number: 604656). The authors would also like to acknowledge the partners in the NanoSim project for their support. The authors would also like to thank Dr Luca Riboldi at NTNU for helping in the understanding of the PSA systems.

References

1. IEA, *Key World Energy Statistics 2017*. 2017.
2. WEO, *World Energy Outlook 2016*. 2016, International Energy Agency.
3. ETP, *Energy Technology Perspectives*. 2017, International Energy Agency.
4. Boot-Handford, M.E., et al., *Carbon capture and storage update.* Energy and Environmental Science, 2014. **7**(1): p. 130-189.
5. Kenarsari, S.D., et al., *Review of recent advances in carbon dioxide separation and capture.* RSC Advances, 2013. **3**(45): p. 22739-22773.
6. Adanez, J., et al., *Progress in chemical-looping combustion and reforming technologies.* Progress in Energy and Combustion Science, 2012. **38**(2): p. 215-282.
7. Ishida, M., D. Zheng, and T. Akehata, *Evaluation of a chemical-looping-combustion power-generation system by graphic exergy analysis.* Energy, 1987. **12**(2): p. 147-154.
8. Rydén, M., A. Lyngfelt, and T. Mattisson, *Synthesis gas generation by chemical-looping reforming in a continuously operating laboratory reactor.* Fuel, 2006. **85**(12-13): p. 1631-1641.
9. Wassie, S.A., et al., *Hydrogen production with integrated CO2 capture in a novel gas switching reforming reactor: Proof-of-concept.* International Journal of Hydrogen Energy, 2017. **42**(21): p. 14367-14379.
10. Zaabout, A., et al., *Experimental Demonstration of a Novel Gas Switching Combustion Reactor for Power Production with Integrated CO2 Capture.* Industrial & Engineering Chemistry Research, 2013. **52**(39): p. 14241-14250.
11. Noorman, S., M. van Sint Annaland, and Kuipers, *Packed Bed Reactor Technology for Chemical-Looping Combustion.* Industrial & Engineering Chemistry Research, 2007. **46**(12): p. 4212-4220.

12. Spallina, V., et al., *Chemical looping reforming in packed-bed reactors: Modelling, experimental validation and large-scale reactor design.* Fuel Processing Technology, 2017. **156**: p. 156-170.
13. Francisco Morgado, J., et al., *Modelling study of two chemical looping reforming reactor configurations: Looping vs. switching.* Powder Technology, 2016.
14. Tang, M., L. Xu, and M. Fan, *Progress in oxygen carrier development of methane-based chemical-looping reforming: A review.* Applied Energy, 2015. **151**.
15. Spallina, V., et al., *Pre-combustion packed bed chemical looping (PCCL) technology for efficient H2-rich gas production processes.* Chemical Engineering Journal, 2016. **294**: p. 478-494.
16. Diglio, G., et al., *Simulation of hydrogen production through chemical looping reforming process in a packed-bed reactor.* Chemical Engineering Research and Design, 2016. **105**: p. 137-151.
17. Yahom, A., et al., *Simulation and thermodynamic analysis of chemical looping reforming and CO2 enhanced chemical looping reforming.* Chemical Engineering Research and Design, 2014. **92**(11): p. 2575-2583.
18. Bischi, A., et al., *Hydrodynamic viability of chemical looping processes by means of cold flow model investigation.* Applied Energy, 2012. **97**: p. 201-216.
19. Pröll, T., et al., *Chemical looping pilot plant results using a nickel-based oxygen carrier.* Oil and Gas Science and Technology, 2011. **66**(2): p. 173-180.
20. Pröll, T., et al., *Syngas and a separate nitrogen/argon stream via chemical looping reforming - A 140 kW pilot plant study.* Fuel, 2010. **89**(6): p. 1249-1256.
21. Ortiz, M., et al., *Hydrogen production by auto-thermal chemical-looping reforming in a pressurized fluidized bed reactor using Ni-based oxygen carriers.* International Journal of Hydrogen Energy, 2010. **35**(1): p. 151-160.
22. Zohrabian, A., et al., *Techno-economic evaluation of an integrated hydrogen and power co-generation system with CO2 capture.* International Journal of Greenhouse Gas Control, 2016. **44**: p. 94-103.
23. Spallina, V., et al., *Techno-economic assessment of membrane assisted fluidized bed reactors for pure H2 production with CO2 capture.* Energy Conversion and Management, 2016. **120**: p. 257-273.
24. Fan, J. and L. Zhu, *Performance analysis of a feasible technology for power and high-purity hydrogen production driven by methane fuel.* Applied Thermal Engineering, 2015. **75**: p. 103-114.
25. Cormos, C.C., L. Petrescu, and A.M. Cormos, *Assessment of hydrogen production systems based on natural gas conversion with carbon capture and storage*, in *Computer Aided Chemical Engineering*. 2014. p. 1081-1086.
26. Martínez, I., et al., *Integrated combined cycle from natural gas with CO2 capture using a Ca-Cu chemical loop.* AIChE Journal, 2013. **59**(8): p. 2780-2794.
27. Mantripragada, H.C. and E.S. Rubin. *Chemical looping for pre-combustion CO2 capture - Performance and cost analysis*. in *Energy Procedia*. 2013.
28. Cormos, C.C., *Evaluation of syngas-based chemical looping applications for hydrogen and power co-generation with CCS.* International Journal of Hydrogen Energy, 2012. **37**(18): p. 13371-13386.
29. Kvamsdal, H.M., K. Jordal, and O. Bolland, *A quantitative comparison of gas turbine cycles with CO2 capture.* Energy, 2007. **32**(1): p. 10-24.
30. Nazir, S., O. Bolland, and S. Amini, *Analysis of Combined Cycle Power Plants with Chemical Looping Reforming of Natural Gas and Pre-Combustion CO2 Capture.* Energies, 2018. **11**(1): p. 147.

31. Nazir, S.M., O. Bolland, and S. Amini, *Full Plant Scale Analysis of Natural Gas Fired Power Plants with Pre-Combustion CO2 Capture and Chemical Looping Reforming (CLR).* Energy Procedia, 2017. **114**: p. 2146-2155.
32. Nazir, S.M., O. Bolland, and S. Amini, *Full Plant Scale Analysis of Natural Gas Fired Power Plants with Pre-Combustion CO2 Capture and Chemical Looping Reforming (CLR).* Energy Procedia, 2017.
33. Cloete, S., et al., *Integration of a Gas Switching Combustion (GSC) system in integrated gasification combined cycles.* International Journal of Greenhouse Gas Control, 2015. **42**(Supplement C): p. 340-356.
34. EBTF, *European best practice guidelines for assessment of CO2 capture technologies. CESAR -project 7th FrameWork Programme. Collaborative Project– GA No. 213569*. 2011.
35. Xu, J. and G.F. Froment, *Methane steam reforming, methanation and water-gas shift: I. Intrinsic kinetics.* AIChE Journal, 1989. **35**(1): p. 88-96.
36. Moayeri, M. and D.L. Trimm, *Effect of carbon deposition on the activity of steam reforming catalysts.* Journal of Applied Chemistry and Biotechnology, 1976. **26**(1): p. 419-424.
37. Snoeck, J.W., G.F. Froment, and M. Fowles, *Steam/CO2 Reforming of Methane. Carbon Filament Formation by the Boudouard Reaction and Gasification by CO2, by H2, and by Steam: Kinetic Study.* Industrial & Engineering Chemistry Research, 2002. **41**(17): p. 4252-4265.
38. Snoeck, J.W., G.F. Froment, and M. Fowles, *Kinetic Study of the Carbon Filament Formation by Methane Cracking on a Nickel Catalyst.* Journal of Catalysis, 1997. **169**(1): p. 250-262.
39. Iliuta, I., et al., *Chemical-looping combustion process: Kinetics and mathematical modeling.* AIChE Journal, 2010. **56**(4): p. 1063-1079.
40. Stull, D.R. and H. Prophet, *JANAF Thermochemical Tables*. 2nd Edition ed. 1971: National Bureau of Standards U.S.
41. Robie, R.A. and B.S. Hemingway, *Thermodynamic properties of minerals and related substances at 298.15 K and 1 bar (10^5 pascals) pressure and at higher temperatures*, in *Bulletin*. 1995.
42. AspenHYSYS, *Aspen HYSYS V8.6 User Guide*. 2017, Aspen Technology Inc., Bedford, Massachusetts, USA.
43. Newsome, D.S., *The Water-Gas Shift Reaction.* Catalysis Reviews, 1980. **21**(2): p. 275-318.
44. Riboldi, L. and O. Bolland, *Overview on Pressure Swing Adsorption (PSA) as CO2 Capture Technology: State-of-the-Art, Limits and Potentials.* Energy Procedia, 2017. **114**(Supplement C): p. 2390-2400.
45. Sircar, S. and T.C. Golden, *Purification of Hydrogen by Pressure Swing Adsorption.* Separation Science and Technology, 2000. **35**(5): p. 667-687.
46. Thermoflow, *Thermoflow Suite V26 User Guide*. 2017, Thermoflow Inc., Southborough, MA, USA.
47. Chiesa, P., G. Lozza, and L. Mazzocchi, *Using Hydrogen as Gas Turbine Fuel.* Journal of Engineering for Gas Turbines and Power, 2005. **127**(1): p. 73-80.
48. Nord, L.O., R. Anantharaman, and O. Bolland, *Design and off-design analyses of a pre-combustion CO2 capture process in a natural gas combined cycle power plant.* International Journal of Greenhouse Gas Control, 2009. **3**(4): p. 385-392.
49. GCCSI, *Global CCS Institute - TOWARD A COMMON METHOD OF COST ESTIMATION FOR CO2 CAPTURE AND STORAGE AT FOSSIL FUEL POWER PLANTS*. 2013.

50. NETL, *Cost Estimation Methodology for NETL Assessments of Power Plant Performance*. 2011.
51. Alibaba. 2017 31 October 2017]; Available from: https://www.alibaba.com/.
52. DOE/NETL, *Cost and Performance Baseline for Fossil Energy Plants*. 2007.
53. Netzer, D., *Alberta Bitumen Processing Integration Study: Final Report*. 2006: publisher not identified.
54. Peters, M.S. and K.D. Timmerhaus, *PLANT DESIGN AND ECONOMICS FOR CHEMICAL ENGINEERS*. Fourth Edition ed. 1991: McGraw-Hill, Inc.
55. Diglio, G., et al., *Techno-economic analysis of sorption-enhanced steam methane reforming in a fixed bed reactor network integrated with fuel cell.* Journal of Power Sources, 2017. **364**(Supplement C): p. 41-51.
56. Gazzani, M., et al., *Using Hydrogen as Gas Turbine Fuel: Premixed Versus Diffusive Flame Combustors.* 2013(55133): p. V002T03A008.
57. Li, L., et al., *A novel oxygen carrier for chemical looping reforming: LaNiO3 perovskite supported on montmorillonite.* Energy, 2017. **131**: p. 58-66.
58. Alirezaei, I., et al., *Application of zirconium modified Cu-based oxygen carrier in chemical looping reforming.* Journal of CO2 Utilization, 2016. **14**: p. 112-121.
59. Wei, G., et al., *Chemical-Looping Reforming of Methane Using Iron Based Oxygen Carrier Modified with Low Content Nickel.* Chinese Journal of Chemistry, 2014. **32**(12): p. 1271-1280.
60. Lozza, G. and P. Chiesa, *Natural Gas Decarbonization to Reduce CO2 Emission From Combined Cycles—Part II: Steam-Methane Reforming.* Journal of Engineering for Gas Turbines and Power, 2000. **124**(1): p. 89-95.